Measurement-based approach to entanglement generation in coupled quantum dots

Avinash Kolli* and Brendon W. Lovett
Department of Materials, Oxford University, Oxford OX1 3PH, United Kingdom

Simon C. Benjamin
Department of Materials, Oxford University, Oxford OX1 3PH, United Kingdom
and Centre for Quantum Technologies, National University of Singapore, 3 Science Drive 2, Singapore 117543

Thomas M. Stace
Department of Physics, University of Queensland, Brisbane, QLD, Australia
(Received 16 January 2008; revised manuscript received 28 May 2008; published 15 January 2009)

The remarkable phenomenon of measurement-induced quantum entanglement has recently been demonstrated between noninteracting atomic systems [D. L. Moehring *et al.*, Nature (London) **449**, 68 (2007)]. In the solid state, the technique may offer a new means of harnessing the strong interactions between neighboring units without the need for precise control over interactions. Recently, we proposed a method for optical parity measurements in a coupled quantum dot system [A. Kolli *et al.*, Phys. Rev. Lett. **97**, 250504 (2006)]. Here we perform a comprehensive analytic and numerical study to determine the feasibility of realizing this method using existing technology. We calculate the effects of possible error sources including nonideal photon detectors, ineffective spin-selective excitation, and dot distinguishability (both spatial and spectral). Furthermore, we present an experimental approach for verifying the success of the parity measurement. We conclude that experimental realization of the process should be feasible immediately.

DOI: 10.1103/PhysRevB.79.035315 PACS number(s): 03.67.Lx, 78.67.Hc, 73.20.Mf, 71.35.Pq

I. INTRODUCTION

Quantum dots (QDs) are semiconductor heterostructures which exhibit strong electron and hole confinement. This leads to a highly discrete level structure, giving rise to many interesting nanotechnological applications, such as quantum information processing (QIP). Such a discrete level structure enables us to identify well-defined effective two-level systems (qubits), which we use to encode our quantum information. A natural qubit is the spin of an excess electron within a quantum dot, which typically exhibits long lifetime (up to milliseconds[1,2]) and coherence times (up to microseconds[3]). Our interest here is in closely separated Foerster coupled quantum dots (CQDs) which exhibit strong optical activity. This scenario may be realized by a pair of vertically stacked self-assembled quantum dots.

As a necessary step toward the eventual goal of practical quantum computation (QC), one must be able to establish entanglement between distinct quantum systems. A natural idea is to exploit the inherent interactions in solid-state systems, for example by permitting periods of free evolution of the coupled systems followed by periods of controlled single-qubit rotations. Early proposals[4] included using the exchange interaction $H=J\hat{S}_1\cdot\hat{S}_2$ to provide the necessary two qubit interaction. However, precise manipulation of the interactions between the spins is needed for such a scheme to work, which appear difficult to achieve in practice.

An alternative method, which we discuss here, is to incorporate measurement as an essential part of the entanglement generation process. The entangling power of measurement was first explored for weakly excited atomic systems,[5] and in the context of linear optical approaches to quantum computation.[6] A number of proposals have since been presented for generating entanglement using optics in solid-state systems. For example, Refs. 7 and 8 propose using single-photon interference to robustly entangle spatially separated matter qubits. A similar idea has also been proposed for entanglement generation, heralded by macroscopic jumps in a fluorescence signal, in atom-cavity-like systems.[9] Measurement-induced entanglement of a pair of atoms has now been experimentally demonstrated.[10]

If we could implement a measurement-based scheme for electron spins then we could do away with the exquisite control over interactions required by the earlier solid-state approaches mentioned above. However, there exists a no-go theorem, which states that it is not possible to achieve an exponential speed-up over classical computation using solely single-electron Hamiltonians and single-spin measurements.[11] Recently, Beenakker *et al.*[12] showed that it is possible to lift this restriction if we look outside the Hilbert space of a spin and exploit the charge degree of freedom. Charge and spin commute, and so we are able to make measurements on the charge without destroying any information that is contained in the spin degrees of freedom. Beenakker *et al.*[12] proceed to show that partial-Bell-state measurements (also known as parity measurements) on the spin states are sufficient to implement a CNOT gate. A number of subsequent papers have proposed specific implementations for these spin-parity measurements. These include a charge tunneling detection method[13] and a charge fluctuation method.[14]

Recently,[15] we proposed a method for optical parity measurements on a pair of coupled quantum dots, exploiting the principle of zero *which-path* information. In this paper we generalize this scheme and perform a comprehensive study of environmental factors. We will begin, in Sec. II by outlining the system and the interactions present. In Sec. III we

will detail the various steps in the spin-parity measurement. We will present results for the operation of the measurement in Sec. IV, and then in Sec. V we will analyze the effect of various error mechanisms, including valence band mixing, and spatial and spectral distinguishability of the two dots. We then proceed to describe a method for verifying the success of our measurement in Sec. VI. Finally, we will give some concluding remarks.

II. COUPLED QUANTUM DOT SYSTEM

In order to develop our coupled model, we will first introduce the structure of a single quantum dot interacting with a laser field. We assume that the dot is n doped such that the valence levels (VL) are completely filled and the only occupied conduction level (CL) is the lowest-lying level. In what follows, we will only consider the top most filled valence states $|J_z=\pm 3/2\rangle$. The CL electron has a spin degree of freedom on which we encode our quantum information: $|0\rangle$ is encoded in the $m_z=-1/2$ state and $|1\rangle$ in $m_z=1/2$. The system is irradiated by a classical σ^+ circularly polarized laser field, resonant with the VL-CL energy gap. An electron-hole pair (exciton) state can be created if a photon's angular momentum of $+\hbar$ can be absorbed; Pauli's exclusion principle means this is only possible when the qubit is in state $|m_z=1/2\rangle=|1\rangle$. This effect is "Pauli Blocking," and it enables us to generate excitons conditioned on the state of the qubit electron. The combined qubit electron/exciton state is a trion, denoted by $|X\rangle$.

When two such doped dots are placed close to each other, there are direct electron spin-spin couplings. However, these are very weak: current experiments place their strengths at less than 1 μeV.[16] We take these interactions to be negligible in comparison to the excitonic interaction that we will exploit. The two primary excitonic couplings that we consider are a static and a dynamic dipole-dipole coupling. The static interaction results in an energy shift V_{XX} of the double trion state and is due to the interdot exciton-exciton dipole interaction. The dynamic coupling, or resonant Foerster interaction V_F, results in an exciton transfer from one dot to the other that is mediated by a virtual photon. This process has been shown, to first-order, to be nonmagnetic and, thus, conserves electron spin.[17] Therefore, in this system the Foerster interaction only couples the $|X1\rangle$ and $|1X\rangle$ states. The Hamiltonian for the coupled QDs is

$$\begin{aligned} H = {} & \omega_0|X\rangle\langle X| \otimes \hat{I} + \omega_0\hat{I} \otimes |X\rangle\langle X| + V_{XX}|XX\rangle\langle XX| \\ & + V_F(|1X\rangle\langle X1| + \text{H.c.}) \\ & + \Omega \cos \omega_l t(|1\rangle\langle X| \otimes \hat{I} + \hat{I} \otimes |1\rangle\langle X| + \text{H.c.}), \end{aligned} \tag{1}$$

where H.c. denotes Hermitian conjugate, ω_0 is the exciton creation energy for both dots (the dots are assumed to be identical), Ω is the time-independent laser coupling (assumed to be the same for both dots), and ω_l is the laser frequency. The energy difference between the $|0\rangle$ and $|1\rangle$ states is negligible on the exciton energy scale.

The Hamiltonian [Eq. (1)] may be decoupled into four subspaces with no interactions between them: $H_{00}=\{|00\rangle\}$, $H_{01}=\{|01\rangle,|0X\rangle\}$, $H_{10}=\{|10\rangle,|X0\rangle\}$, and $H_{11}=\{|11\rangle,|X1\rangle,|X1\rangle,|XX\rangle\}$. Let us look more closely at the Hamiltonian for the last of these subspaces. We rewrite this in basis of the eigenstates when $\Omega=0$, which are $|11\rangle$, $|\psi_+\rangle=\frac{1}{\sqrt{2}}(|1X\rangle+|X1\rangle)$, $|\psi_-\rangle=\frac{1}{\sqrt{2}}(|1X\rangle-|X1\rangle)$, and $|XX\rangle$. The degeneracy of the $|\psi_-\rangle$ and $|\psi_+\rangle$ levels is lifted by the Foerster interaction, resulting in two states each containing a delocalized exciton. In this basis the Hamiltonian is, after reintroducing a finite Ω,

$$\begin{aligned} H_{11} = {} & (\omega_0 + V_F)|\psi_+\rangle\langle\psi_+| + (\omega_0 - V_F)|\psi_-\rangle\langle\psi_-| + (2\omega_0 + V_{XX}) \\ & \times|XX\rangle\langle XX| + \Omega' \cos \omega_l t(|11\rangle\langle\psi_+| + |\psi_+\rangle\langle XX| + \text{H.c.}). \end{aligned} \tag{2}$$

The only dipole allowed transitions in this subspace are between $|11\rangle$ and $|\psi_+\rangle$, and between $|\psi_+\rangle$ and $|XX\rangle$, with a coupling strength of $\Omega'=\sqrt{2}\Omega$. The level structure for all four subspaces is shown in Fig. 1.

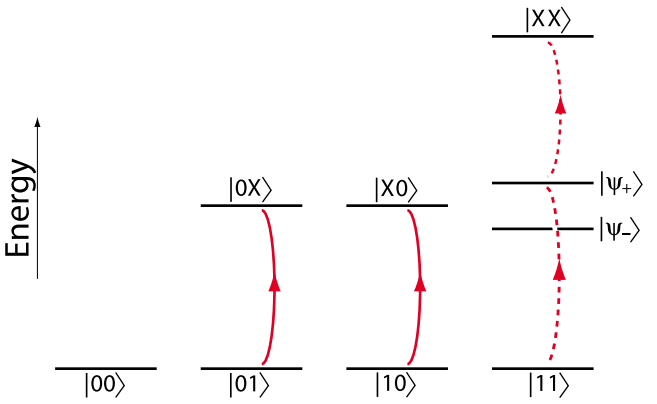

FIG. 1. (Color online) Energy level diagram for the coupled quantum dot structure. Resonant transitions are denoted by the solid lines, while nonresonant transitions by dotted lines.

III. SPIN-PARITY MEASUREMENT

The parity measurement protocol consists of two steps: excitation followed by monitored relaxation. In the excitation we aim to transfer the population of the states from the computational basis into the excitonic levels in the odd-parity $\{|01\rangle,|10\rangle\}$ subspace, while retaining the population of the even-parity $\{|00\rangle,|11\rangle\}$ states in the ground levels. We can achieve this by exciting the coupled dots with a pulsed laser tuned to energy ω_0. By referring to Fig. 1 and Eqs. (1) and (2), we can see that such a laser excites transitions within the $|01\rangle$ and $|10\rangle$ subspaces. The $|11\rangle$ state is not excited to first order if

$$|V_F|,|V_{XX}| \gg |\Omega'|/2 \tag{3}$$

since the laser is off resonance with the excited levels in this space, and $|00\rangle$ is of course optically inactive.

Suppose we have an initial state

$$|\psi_0\rangle = \alpha_{00}|00\rangle + \alpha_{01}|01\rangle + \alpha_{10}|10\rangle + \alpha_{11}|11\rangle. \tag{4}$$

After an excitation π pulse, our state is $|\psi\rangle=\alpha_{00}|00\rangle+\alpha_{01}|0X\rangle+\alpha_{10}|X0\rangle+\alpha_{11}|11\rangle$. We next enter a period of moni-

toring the system for decay photons. Assuming perfect detection, the state of the system is projected into the odd-parity subspace if a photon is detected, and into the even-parity subspace if a photon is not detected. Importantly, we only distinguish between the two parity subspaces without distinguishing states within the same subspace. We can represent the action of the measurement in terms of projection operators for the two desired outcomes,

$$P_O = |\psi_{\text{odd}}\rangle\langle\psi_{\text{odd}}| = |01\rangle\langle 01| + |10\rangle\langle 10|,$$

$$P_E = |\psi_{\text{even}}\rangle\langle\psi_{\text{even}}| = |00\rangle\langle 00| + |11\rangle\langle 11|. \quad (5)$$

As mentioned earlier, we must not be able to distinguish between states within the same subspace. Therefore, it is important throughout the radiative relaxation that there is no information gained about the source of the photon that is emitted. There are many ways in which this condition can be compromised—for example, spatial and spectral distinguishability of photon emissions from the different dots. Our system will also have imperfect detectors; in Sec. IV we will begin to look at these potential sources of error.

IV. CONDITIONAL DYNAMICS WITH IMPERFECT DETECTORS

To model the monitored radiative relaxation we use the quantum trajectories formalism.[18–20] The conditional master equation (CME) describing n-monitored relaxation channels is

$$d\rho_c = -i[H,\rho_c]dt + \sum_j^n \{\eta_j Tr(\mathcal{J}[c_j]\rho_c)\rho_c + (1-\eta_j)\mathcal{J}[c_j]\rho_c - \mathcal{A}[c_j]\rho_c\}dt + \left\{\frac{\mathcal{J}[c_j]\rho_c}{Tr(\mathcal{J}[c_j]\rho_c)} - \rho_c\right\}dN_j, \quad (6)$$

where ρ_c is the density matrix of the system, H is the system Hamiltonian in the interaction picture, c_j is the Lindblad operator through which the system couples to the measurement channel j, $\mathcal{J}[c_j]$ is the jump superoperator, which projects out the component of the state that is consistent with a detection from channel j and is defined as $\mathcal{J}[c_j]\rho_c = c_j^\dagger \rho_c c_j$. $\mathcal{A}[c_j]$ is defined to be $\mathcal{A}[c_j]\rho_c = \frac{1}{2}(c_j^\dagger c_j \rho_c + \rho_c c_j^\dagger c_j)$; η_j is the efficiency of the detector that monitors emission into channel j. $dN_j(t)$ is the classical stochastic increment taking the values $\{0,1\}$, which denotes the number of photons detected in channel j in the interval $t, t+dt$.

Between quantum jumps, when $dN(t)=0$, Eq. (6) is equivalent to the linear, unnormalized CME,

$$\dot{\tilde{\rho}} = -i[H,\tilde{\rho}] + \sum_j^n \{(1-\eta_j)\mathcal{J}[c_j]\tilde{\rho} - \mathcal{A}[c_j]\tilde{\rho}\}, \quad (7)$$

where $\rho_c = \tilde{\rho}/Tr(\tilde{\rho})$.

Assuming that condition (3) is satisfied, there are no excitons in the even subspace. Thus we need only consider one channel defined by the Lindblad operator $c = \sqrt{\Gamma_X}(|01\rangle\langle 0X| + |10\rangle\langle X0|)$. Furthermore, the odd space only contains a single excitation, and thus, we can model the dynamics in two steps: a period of continuous evolution followed by a potential single quantum jump due to the photon detection event.

TABLE I. Table of relevant parameters for the coupled quantum dot system.

Parameters	Value
V_F	0.85 meV
V_{XX}	5 meV
ω_0	2 eV
Ω	0.1 meV
τ_X	1 ns
Γ_X	4 μeV

Suitable parameters for an immediate future experiment are displayed in Table I.[21–24] The laser driving strength, Ω, is chosen such that population within the excited states in the 11 subspace is only 1%.

For an initial state [Eq. (4)], and using Eq. (7), we find that the probability p_E that we are in the even-parity subspace at a time t after excitation is

$$p_E(t) = \frac{\alpha_{00}^2 + \alpha_{11}^2}{1 + \eta(\alpha_{01}^2 + \alpha_{10}^2)(e^{-\Gamma_X t} - 1)}. \quad (8)$$

In order to increase this probability, it makes sense to wait long enough that we can be sure that if a photon has not yet been emitted, it is not likely to be emitted in future. This amounts to waiting for a time $t \gg 1/\Gamma_X$. Then the fidelity of projection into the even subspace is

$$F_E = \frac{\alpha_{00}^2 + \alpha_{11}^2}{(1-\eta)(\alpha_{01}^2 + \alpha_{10}^2) + (\alpha_{00}^2 + \alpha_{11}^2)}. \quad (9)$$

When a photon is detected (and ignoring typically negligible detector dark counts) the fidelity of projection into the odd subspace is $F_O = 1$.

The success of our two-step parity measurement is strongly dependent on detector efficiency, and can become quite poor for typical values of η. However, by repeating the spin-parity measurement one or more times, it is possible to obtain improved fidelities. On each round of the repeated measurement, we gain greater confidence that we have successfully projected into the even subspace, rather than missing every emitted photon. To analyze this we write the effect of the spin-parity measurement when no photon is measured in the quantum operation formalism.[25] The action of a general quantum operation can be written as

$$\rho \to \mathcal{E}(\rho) = \sum_k \tilde{E}_k \rho \tilde{E}_k^\dagger, \quad (10)$$

where the $\tilde{E}_k$ are the Krauss projection operators, which must satisfy the normalization condition $\Sigma_k \tilde{E}_k^\dagger \tilde{E}_k = 1$. For our particular example, a single operation of the spin-parity measurement will yield

$$\rho \to \mathcal{E}(\rho) = \frac{c_O \tilde{E}_O \rho \tilde{E}_O^\dagger + c_E \tilde{E}_E \rho \tilde{E}_E^\dagger}{Tr[c_O \tilde{E}_O \rho \tilde{E}_O^\dagger + c_E \tilde{E}_E \rho \tilde{E}_E^\dagger]}, \tag{11}$$

where the unnormalized Krauss operators, defined as $\tilde{E}_{O,E} = P_{O,E} = |\psi_{O,E}\rangle\langle\psi_{O,E}|$, are the projectors onto the odd and even-parity subspaces, respectively, and the coefficients are chosen in a self-consistent manner: $c_E = 1$ and $c_O = (1-\eta)$. The denominator in this expression ensures that we satisfy the normalization condition.

When the measurement is repeated r times, the overall quantum operation is given by

$$\rho \to \mathcal{E}[\mathcal{E}(\rho)] = \frac{c_O^r \tilde{E}_O \rho \tilde{E}_O^\dagger + c_E^r \tilde{E}_E \rho \tilde{E}_E^\dagger}{Tr[c_O^r \tilde{E}_O \rho \tilde{E}_O^\dagger + c_E^r \tilde{E}_E \rho \tilde{E}_E^\dagger]}. \tag{12}$$

The fidelity of correctly projecting into the even subspace is therefore given by

$$F_E^r = \frac{Tr[c_E^r \tilde{E}_E \rho \tilde{E}_E^\dagger]}{Tr[c_O^r \tilde{E}_O \rho \tilde{E}_O^\dagger + c_E^r \tilde{E}_E \rho \tilde{E}_E^\dagger]} = \frac{(\alpha_{00}^2 + \alpha_{11}^2)}{(1-\eta)^r(\alpha_{01}^2 + \alpha_{10}^2) + (\alpha_{00}^2 + \alpha_{11}^2)}. \tag{13}$$

For all nonzero detector efficiencies, in the limit $r \to \infty$ the term $(1-\eta)^r$ will tend to zero. We can, therefore, expect a unit fidelity for every input state in this limit.

Let us now look at the average fidelity for all input states as a function of r. Owing to the normalization condition $\alpha_{00}^2 + \alpha_{01}^2 + \alpha_{10}^2 + \alpha_{11}^2 = 1$, we write the four coefficients in terms of four-dimensional hyperspherical polar coordinates,

$$\alpha_{00} = \sin\phi_1 \sin\phi_2 \cos\phi_3,$$

$$\alpha_{01} = \cos\phi_1,$$

$$\alpha_{10} = \sin\phi_1 \cos\phi_2,$$

$$\alpha_{11} = \sin\phi_1 \sin\phi_2 \sin\phi_3, \tag{14}$$

and the area element is given by

$$dA = \sin^2\phi_1 \sin\phi_2 d\phi_1 d\phi_2 d\phi_3. \tag{15}$$

The resulting integral is

$$\bar{F}_E^r = \int_0^\pi d\phi_1 \sin^2\phi_1 \int_0^\pi d\phi_2 \sin\phi_2 \int_0^{2\pi} d\phi_3 F_E^r. \tag{16}$$

This integration is performed numerically and the resulting averaged fidelity as a function of η can be seen in Fig. 2. We clearly see a convergence, as $r \to \infty$, of the average fidelity to unity for all nonzero detection efficiencies. Thus, by simply repeating the measurement, we are able to overcome the inherent problems of lossy detectors.

V. CORRECTIONS TO MODEL

A. Valence-band mixing

The Pauli blocking mechanism, crucial to the success of the excitation step, is valid only in the case of no light-heavy hole mixing, which is only true in very limited cases.[26] Usually the hole eigenstates are composed of mixtures of light hole ($|J_z = \pm 1/2\rangle$) and heavy hole ($|J_z = \pm 3/2\rangle$) states.[27] The mixing is characterized by a factor ϵ. This results in two families of eigenstates: one with predominantly light hole character and one with predominantly heavy hole character. The latter tend to be the topmost valence levels and are[17]

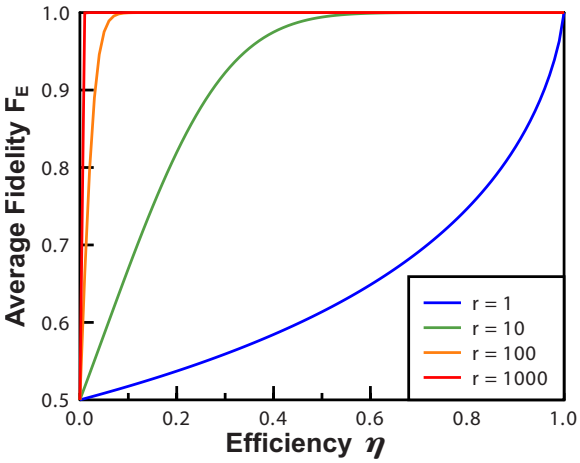

FIG. 2. (Color online) The averaged fidelities $\bar{F}_E$ as a function of detector efficiency.

$$|h_+\rangle = \sqrt{1-\epsilon^2}|J_z = +3/2\rangle + \epsilon|J_z = -1/2\rangle,$$

$$|h_-\rangle = \sqrt{1-\epsilon^2}|J_z = -3/2\rangle + \epsilon|J_z = +1/2\rangle. \tag{17}$$

On applying the σ^+ polarized laser field, it is now possible to generate excitons from both the $|0\rangle = |m_z = -1/2\rangle$ and $|1\rangle = |m_z = +1/2\rangle$ electron states. The resulting exciton-laser field coupling Hamiltonian is

$$H_{\sigma^+} = \cos[\omega_L t](|1\rangle\langle X_-| + \tilde{\epsilon}|0\rangle\langle X_+| + \text{H.c.}), \tag{18}$$

where the trion levels are $|X_{+,-}\rangle = |S_{\uparrow\downarrow}\rangle \otimes |h_{+,-}\rangle$. The modified mixing angle is $\tilde{\epsilon} = \epsilon \frac{l_{lh}}{\sqrt{3} l_{hh}}$ and $l_{lh,hh}$ are characteristic lengths associated with the overlap of the electron and the lh, hh Bloch functions (see Ref. 17).

The mixing also induces a Foerster interaction that couple other single exciton levels,

$$H_F = M_{hh,hh}(|0X_+\rangle\langle X_+0| + |1X_-\rangle\langle X_-1|) + \frac{2M_{lh,hh}\epsilon}{\sqrt{3}}(|0X_-\rangle\langle X_+1| + |1X_+\rangle\langle X_-0|) + \text{H.c.}, \tag{19}$$

where $M_{i,j}$ are the matrix elements for the transitions induced by the Foerster interaction and i and j denote the different initial and final hole states, respectively.

The Hamiltonian for the coupled quantum dots is now

$$H = \omega_0(|X_+\rangle\langle X_+| + |X_-\rangle\langle X_-|) \otimes I + \omega_0 I \otimes (|X_+\rangle\langle X_+| + |X_-\rangle\langle X_-|) + H_F + H_{\sigma^+} + \sum_{\mu,\nu \in \{X_-,X_+\}} V_{XX}|\mu\nu\rangle\langle\mu\nu|. \tag{20}$$

With the inclusion of hole mixing *each* decoupled subspace will now have two single excitonic levels and a biex-

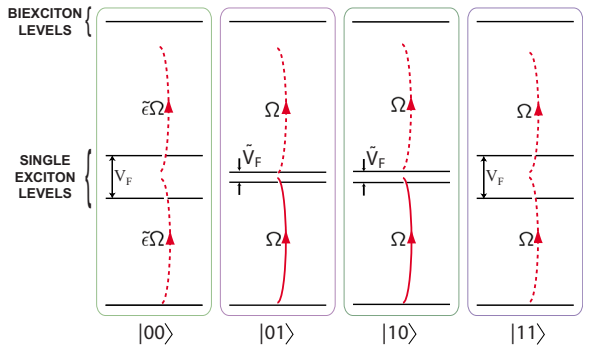

FIG. 3. (Color online) The effect of hole mixing on the level structure of the coupled quantum dot system. The two Foerster interaction terms are $V_F=M_{hh,hh}$ and $\tilde{V}_F=2\tilde{\epsilon}M_{lh,hh}$. Once again, far-off resonant transitions are denoted by dashed lines and near resonant transitions by solid lines.

citon level, and this is illustrated in Fig. 3. We now discuss whether we can still perform the parity projection in this more complex situation.

First, we must ensure that transitions to excitonic levels in the even subspace remain suppressed. Condition (3) is still valid for suppressing transitions from $|11\rangle$. Meanwhile, the couplings to the excitonic levels from the $|00\rangle$ state are reduced by the mixing factor $\tilde{\epsilon}$, and so condition (3) is also sufficient to suppress these transitions.

Second, transitions within the odd subspace must only occur between the zero- and single-exciton levels. Our measurement replies on the detection of a single photon: on detection of the photon any population in the biexciton level will be projected into the single excitonic levels, and this must be avoided.

The dynamics is identical for the $|01\rangle$ and $|10\rangle$ subspaces so we will concentrate only on the levels within the $|01\rangle$ subspace. In the basis $\{|01\rangle,|0X_-\rangle,|X_+1\rangle,|X_+X_-\rangle\}$ the Hamiltonian is

$$H=\begin{pmatrix} 0 & \Omega/2 & \tilde{\epsilon}\Omega/2 & 0 \\ \Omega/2 & \delta & \tilde{V}_F & \tilde{\epsilon}\Omega/2 \\ \tilde{\epsilon}\Omega/2 & \tilde{V}_F & \delta & \Omega/2 \\ 0 & \tilde{\epsilon}\Omega/2 & \Omega/2 & 2\delta+V_{XX} \end{pmatrix}, \tag{21}$$

where $\delta=\omega_0-\omega_L$ and $\tilde{V}_F=2\tilde{\epsilon}M_{lh,hh}$. We follow the evolution of the four levels within this subspace over the course of the excitation pulse. We are interested in the populations of the $|01\rangle$ and $|X_+X_-\rangle$ at the end of the excitation pulse, and so in Fig. 4 we plot the evolution of these populations over time for a range of realistic mixing factors.

We see that, as a result of the strong biexciton shift V_{XX}, the population build-up of the $|X_-X_+\rangle$ is suppressed for a range of realistic mixing factors. For mixing factors up to $\epsilon=0.05$ the computational states $|01\rangle$ and $|10\rangle$ are also effectively depopulated—and so we conclude that hole mixing is not a serious problem for the parity projection.

B. QD spatial separation

The two quantum dots that form our CQD structure are naturally spatially separated. Typically the separation would be more than an order of magnitude smaller than the relevant optical wavelength. However as has been mentioned in Sec. III, any source of distinguishability will affect the coherence between the odd-parity states upon detection of a photon. To analyze this effect we derive a new CME describing the detection step, which includes the effects of spatial separation.

This is done in three stages: first we derive a Markovian master equation from a microscopic Hamiltonian describing the full dynamics of the system and bath. We then define a jump superoperator, which describes the evolution of the system upon a detection event. Finally we are able to identify a CME by imposing the condition that the time-averaged CME is equal to the master equation derived in the first step.

The Markovian master equation is derived from the following integrodifferential equation:

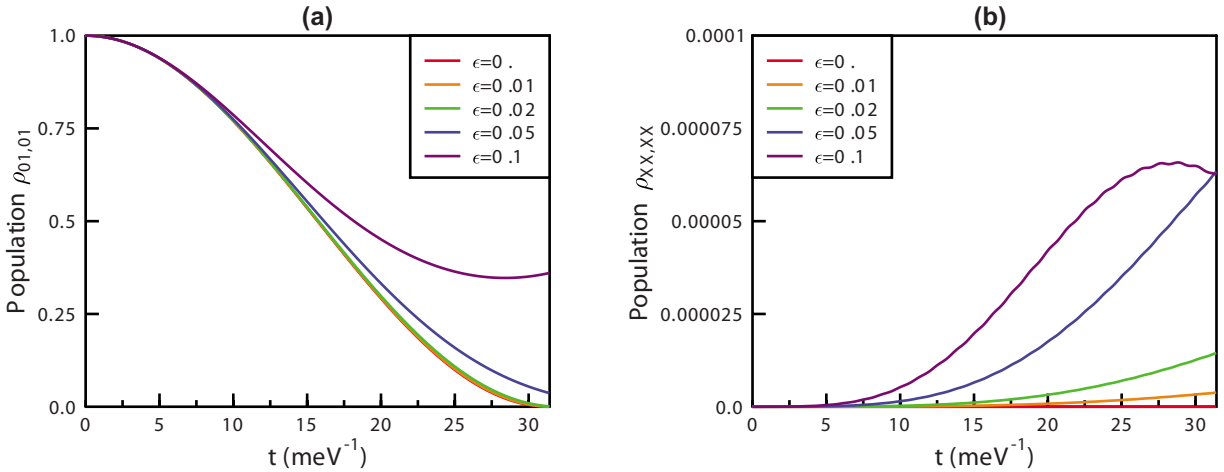

FIG. 4. (Color online) Populations of (a) $|01\rangle$ and (b) $|X_-X_+\rangle$ levels through the duration of the excitation pulse. The parameters are chosen as follows: $M_{hh,hh}=M_{lh,hh}=V_F$ and $l_{hh}=l_{lh}$. The laser is tuned to the exciton creation energy ω_0 so that $\delta=0$.

$$\dot{\rho}(t) = -\int_0^\infty d\tau Tr_{\rm ph}\{\{H_I(t),[H_I(t-\tau),\rho(t)\otimes\rho_{\rm ph}]\}\}, \quad (22)$$

where $H_I(t)$ is the microscopic Hamiltonian in the interaction picture, $\rho(t)$ is the density matrix for the system, and $\rho_{\rm ph}$ is the density matrix for the photon bath. If our interaction Hamiltonian is of the general form,

$$H_I = \sum_i A_i(t)\otimes B_i(t), \quad (23)$$

then we may write the master equation in the Born-Markov approximation as

$$\dot{\rho}(t) = -\int_0^\infty d\tau \sum_{\alpha,\beta} C_{\alpha,\beta}(\tau)[A_\alpha^\dagger(t)A_\beta(t-\tau)\rho(t) - A_\beta(t-\tau)\rho(t)A_\alpha^\dagger(t)] + \text{H.c.}, \quad (24)$$

where $C_{\alpha,\beta}(\tau)=Tr_{\rm ph}[B_\alpha^\dagger(\tau)B_\beta(0)\rho_{\rm ph}]$ is the environment correlation function.

For our case of two quantum dots coupled to a photon bath, the microscopic Hamiltonian is

$$H = H_{\rm CQD} + H_{\rm ph} + H_{\rm int} \quad (25)$$

with

$$H_{\rm CQD} = \omega_0(c_{X0}^\dagger c_{X0} + c_{0X}^\dagger c_{0X}),$$

$$H_{\rm ph} = \sum_{\mathbf{k}} \omega_{\mathbf{k}} a_{\mathbf{k}}^\dagger a_{\mathbf{k}},$$

$$H_{\rm int} = \sum_{\mathbf{k}} f(\mathbf{k}) a_{\mathbf{k}} e^{i\mathbf{k}.\mathbf{r}}(c_{X0}^\dagger + e^{i\mathbf{k}.\Delta\mathbf{r}}c_{0X}^\dagger) + \text{H.c.} \quad (26)$$

$c_{X0,0X}$ represents the annihilation operator for an exciton on dot A, B, respectively, and $a_{\mathbf{k}}$ is the annihilation operator for a quantum of the electric field. $\mathbf{k}$ is the wave vector for the electric field, $f(\mathbf{k})=(\hat{\mu}.\hat{\sigma}_{\mathbf{k}})\epsilon_{\mathbf{k}}$ where $\hat{\mu}$ is the dipole moment vector for each qubit, $\hat{\sigma}_{\mathbf{k}}$ is the polarization vector for the electric field, and $\epsilon_{\mathbf{k}}$ is the energy of a mode $\mathbf{k}$ of the electric field. Finally, $\Delta\mathbf{r}$ is the center-to-center separation of the two quantum dots.

We first transform to the interaction picture defined by $H_0=H_{\rm CQD}+H_{\rm ph}$,

$$H_I = \sum_{\mathbf{k}} f(\mathbf{k}) e^{i\mathbf{k}.\mathbf{r}} e^{i(\omega_k-\omega_0)t} a_{\mathbf{k}}(c_{X0}^\dagger + e^{i\mathbf{k}.\Delta\mathbf{r}}c_{0X}^\dagger) + \text{H.c.} \quad (27)$$

We now proceed to calculate the master equation using Eqs. (23) and (24). We must first identify the system and bath operators, $A_i(t)$ and $B_i(t)$, respectively. We choose

$$A_{\mathbf{k}}^\dagger(t) = f(\mathbf{k})e^{i\mathbf{k}.\mathbf{r}}(c_{X0}^\dagger + e^{i\mathbf{k}.\Delta\mathbf{r}}c_{0X}^\dagger)e^{i\omega_0 t} = P_{\mathbf{k}}^\dagger e^{i\omega_0 t},$$

$$B_{\mathbf{k}}^\dagger(t) = a_{\mathbf{k}} e^{-i\omega_{\mathbf{k}} t}. \quad (28)$$

The master equation then becomes

$$\dot{\rho}(t) = -2\pi\sum_{\mathbf{k}} \frac{1}{2}[1+\tilde{N}(\omega_{\mathbf{k}})][P_{\mathbf{k}}^\dagger P_{\mathbf{k}}\rho(t) - 2P_{\mathbf{k}}\rho(t)P_{\mathbf{k}}^\dagger + \rho(t)P_{\mathbf{k}}^\dagger P_{\mathbf{k}}]\delta(\omega_0-\omega_{\mathbf{k}}) + \frac{1}{2}\tilde{N}(\omega_{\mathbf{k}})[P_{\mathbf{k}}P_{\mathbf{k}}^\dagger\rho(t) - 2P_{\mathbf{k}}^\dagger\rho(t)P_{\mathbf{k}} + \rho(t)P_{\mathbf{k}}P_{\mathbf{k}}^\dagger]\delta(\omega_0-\omega_{\mathbf{k}}), \quad (29)$$

where $\tilde{N}(\omega_{\mathbf{k}})=(1-e^{-\omega_k/k_BT})^{-1}$ is the occupation number of mode k. As $k_BT \ll \omega_k$ we may assume that $\tilde{N}(\omega_{\mathbf{k}})=0$, and so the master equation back in the Schrödinger picture is

$$\dot{\rho} = -i[H,\rho] + \sum_{\mathbf{k}}\left(P_{\mathbf{k}}\rho P_{\mathbf{k}}^\dagger - \frac{1}{2}\{P_{\mathbf{k}}^\dagger P_{\mathbf{k}}\rho + \rho P_{\mathbf{k}}^\dagger P_{\mathbf{k}}\}\right)\delta(\omega_0-\omega_k). \quad (30)$$

Our detection model is simply a single-photon detection so we now can define our jump superoperator as

$$\mathcal{J}[\rho] = \sum_{\mathbf{k}'} P_{\mathbf{k}'}\rho P_{\mathbf{k}'}^\dagger \delta(\omega_0-\omega_k), \quad (31)$$

where the $\mathbf{k}'$ vector runs over the solid angle covered by the detector. It is assumed for simplicity that the detector covers the full solid angle, and also assuming an overall detector inefficiency η, the stochastic master equation becomes

$$\dot{\tilde{\rho}} = -i[H,\tilde{\rho}] + \sum_{\mathbf{k}}\left\{(1-\eta)P_{\mathbf{k}}\tilde{\rho}P_{\mathbf{k}}^\dagger - \frac{1}{2}\{P_{\mathbf{k}}^\dagger P_{\mathbf{k}},\tilde{\rho}\}\right\}\delta(\omega_0-\omega_k). \quad (32)$$

Performing the sum over all modes, we obtain

$$\dot{\tilde{\rho}} = -i[H,\tilde{\rho}] + (1-\eta)\mathcal{J}\tilde{\rho} - \mathcal{A}\tilde{\rho}, \quad (33)$$

where

$$\mathcal{J}\tilde{\rho} = \Gamma_1[c_{X0}\rho c_{X0}^\dagger + 3f(k_0\Delta r)(c_{X0}\rho c_{0X}^\dagger + c_{0X}\rho c_{X0}^\dagger) + c_{0X}\rho c_{0X}^\dagger], \quad (34)$$

$$\mathcal{A}\tilde{\rho} = \Gamma_1[c_{X0}^\dagger c_{X0}\rho + \rho c_{X0}^\dagger c_{0X} + c_{0X}^\dagger c_{0X}\rho + \rho c_{0X}^\dagger c_{0X}], \quad (35)$$

and

$$f(\alpha) = \frac{2\alpha\cos(\alpha) + (\alpha^2-2)\sin(\alpha)}{\alpha^3}. \quad (36)$$

The function $3f(k_0\Delta r)$ characterizes the decohering effect of distinguishable photons. It takes a value of unity for perfectly indistinguishable dots, and then Eq. (33) reduces to Eq. (7). Stacked self-assembled QDs have separations of the order 5 nm,[23] while the typical exciton creation energy is $\omega_0=2$ eV. This gives a value of $3f(k_0\Delta r)=0.99925$, and we can conclude that spatial separation has a negligible effect on the successful operation of the parity measurement.

C. Detuning of QD excitonic energy levels

We have up to this point neglected any inhomogeneity in the underlying structure of the two dots in our coupled system. However, in practice we must expect a certain degree of

inhomogeneity: for example, due to the growth technique self-assembled vertically coupled quantum dots will tend to have different sizes. This will result in differences in the confining potentials for the two dots, which in turn will impact on the exciton creation energies, and the overlap integrals, which determine the coupling with the laser field. For our parity measurement, the most important effect will come from the detuning or nonresonance of the exciton creation energies for the two dots. This will affect both our ability to perform the excitation step and also the ability to retain coherence when we measure a photon. These effects will be analyzed in this section.

1. Excitation pulse

To begin, let us concentrate on the excitation step. As with the hole mixing, we have two primary concerns: first we must maintain the population of the even subspace within the computational ground states, and second we must ensure that the populations within the odd subspace are completely transferred to the excitonic levels.

Let us initially focus on the first issue. The Hamiltonian for the 11 subspace, written in the basis $\{|11\rangle,|1X\rangle,|X1\rangle,|XX\rangle\}$, is now

$$H = \begin{pmatrix} 0 & \Omega/2 & \Omega/2 & 0 \\ \Omega/2 & \delta_B & V_F & \Omega/2 \\ \Omega/2 & V_F & \delta_A & \Omega/2 \\ 0 & \Omega/2 & \Omega/2 & \delta_A + \delta_B + V_{XX} \end{pmatrix}, \tag{37}$$

where $\delta_{A,B}=\omega_{A,B}-\omega_L$.

As before, we begin by transforming the Hamiltonian into a basis of $\Omega=0$ eigenstates. The single exciton subspace is transformed using the following:

$$\begin{pmatrix} |1X\rangle \\ |X1\rangle \end{pmatrix} = \begin{pmatrix} \cos\theta & -\sin\theta \\ \sin\theta & \cos\theta \end{pmatrix} \begin{pmatrix} |\psi_-\rangle \\ |\psi_+\rangle \end{pmatrix}, \tag{38}$$

where $\theta=1/2\arctan[2V_F/(\delta_A-\delta_B)]$ is the mixing angle for the two states $\{|1X\rangle,|X1\rangle\}$, and $\{|\psi_-\rangle,|\psi_+\rangle\}$ are the new eigenstates. Reintroducing the laser coupling, we find that the Hamiltonian in the new basis $\{|11\rangle,|\psi_-\rangle,|\psi_+\rangle,|XX\rangle\}$ is

$$H = \begin{pmatrix} 0 & \Omega_-/2 & \Omega_+/2 & 0 \\ \Omega_-/2 & \delta'_B & 0 & \Omega_-/2 \\ \Omega_+/2 & 0 & \delta'_A & \Omega_+/2 \\ 0 & \Omega_-/2 & \Omega_+/2 & \delta_A + \delta_B + V_{XX} \end{pmatrix}, \tag{39}$$

where $\Omega_\pm=\Omega(\cos\theta\pm\sin\theta)$ and

$$\delta'_A = \delta_A \cos^2\theta + \delta_B \sin^2\theta + V_F \sin 2\theta,$$

$$\delta'_B = \delta_A \sin^2\theta + \delta_B \cos^2\theta - V_F \sin 2\theta. \tag{40}$$

To suppress any transitions to the excitonic levels, we require that

$$\Omega_\pm/2 \ll \delta'_A, \delta'_B, \delta_A + \delta_B + V_{XX}. \tag{41}$$

For both limits of small detuning ($\delta=\delta_A-\delta_B<2V_F$) and large detuning ($\delta=\delta_A-\delta_B>2V_F$), this condition is satisfied.

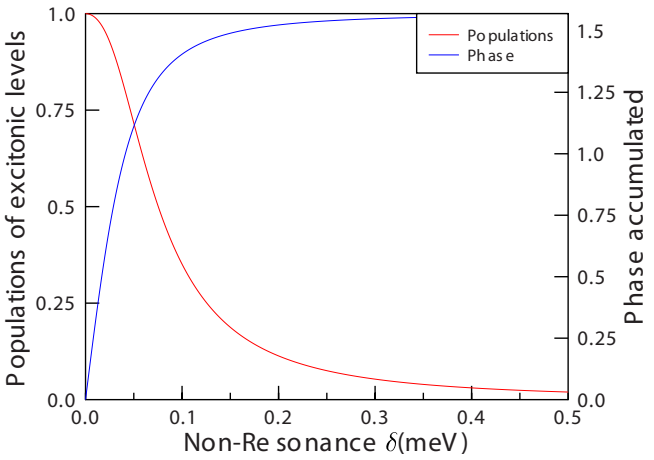

FIG. 5. (Color online) Plot of the population of the single excitonic levels and the phase between them at the end of the excitation step as a function of the detuning of the two QDs.

Let us now turn our attention to the dynamics within the odd subspace during the excitation phase. For a successful outcome, we must effect the same population transfer into the exciton levels for both the $|01\rangle$ and $|10\rangle$ initial states. The joint Hamiltonian for these two subspaces, in the rotating frame, is

$$H = \begin{pmatrix} 0 & \Omega/2 & 0 & 0 \\ \Omega/2 & \delta_A & 0 & 0 \\ 0 & 0 & 0 & \Omega/2 \\ 0 & 0 & \Omega/2 & \delta_B \end{pmatrix}. \tag{42}$$

To achieve equal population transfer to the $|0X\rangle$ and $|X0\rangle$ the laser is tuned to the midpoint between the two excitonic levels: $\delta_A=-\delta_B=\delta=(\omega_A-\omega_B)/2$. The maximum population of the excitonic levels is given by $\Omega^2/(\Omega^2+\delta^2)$ and is found at a time of $\tau_\pi=\pi/2\sqrt{\Omega^2+\delta^2}$. For $\Omega\gg\delta$ we can achieve the required π pulse for each odd-parity state. However, we must also ensure that the coherence between the $|01\rangle$ and $|10\rangle$ states is preserved as we transfer the population to the excited states. Since the levels are not resonant, a net phase difference can be accumulated between them by the end of this excitation pulse. The variation in this phase is shown, along with the population of the excitonic states, in Fig. 5 as a function of detuning. The figure seems to show that we require very similar dots to ensure a successful excitation pulse. However, if the phase accumulated is known, it is possible to correct for at the end of the measurement using single-qubit operations.

2. Detection

We next discuss the effect of detuning on the detection process. To analyze this we will derive a master equation from first principles describing the relaxation process. From here we will proceed to identify the relevant jump operator associated with the detection of a photon and the resulting CME governing the dynamics of the system until the measurement occurs.

We start with a microscopic Hamiltonian describing the coupled quantum dots, the photon bath, and also the coupling between these two systems,

$$H = H_{\mathrm{CQD}} + H_{\mathrm{ph}} + H_{\mathrm{int}}, \tag{43}$$

where

$$H_{\mathrm{CQD}} = \omega_A c_{X0}^{\dagger} c_{X0} + \omega_B c_{0X}^{\dagger} c_{0X},$$

$$H_{\mathrm{ph}} = \sum_{\mathbf{k}} \omega_{\mathbf{k}} a_{\mathbf{k}}^{\dagger} a_{\mathbf{k}},$$

$$H_{\mathrm{int}} = \sum_{\mathbf{k}} g_{\mathbf{k}} a_{\mathbf{k}}^{\dagger} (c_{0X} + c_{X0}) + \mathrm{H.c.}, \tag{44}$$

where $g_{\mathbf{k}}$ is the photon-exciton coupling constant and is assumed to remain identical for both dots (any discrepancy can absorbed into the total decay rates Γ_A and Γ_B). Note that in contrast to Eq. (27), here we are neglecting spatial separation but accounting for frequency discrepancy.

We begin by transforming into the interaction picture, defined by $H_0 = H_{\mathrm{CQD}} + H_{\mathrm{ph}}$. The resulting interaction Hamiltonian is

$$H_I = \sum_{\mathbf{k}} g_{\mathbf{k}} a_{\mathbf{k}}^{\dagger} (e^{i(\omega_{\mathbf{k}} - \omega_A)t} c_{X0} + e^{i(\omega_{\mathbf{k}} - \omega_B)t} c_{0X}) + \mathrm{H.c.} \tag{45}$$

We proceed as before [Eqs. (23) and (24)] by defining the system and environment eigenoperators $A_i(t)$ and $B_i(t)$, respectively,

$$A_{\mathbf{k}}^{\dagger}(t) = g(\mathbf{k})(e^{i\omega_A t} c_{X0}^{\dagger} + e^{i\omega_B t} c_{0X}^{\dagger}),$$

$$B_{\mathbf{k}}^{\dagger}(t) = a_{\mathbf{k}} e^{-i\omega_{\mathbf{k}} t}. \tag{46}$$

Assuming that we are operating at zero temperature, we obtain the following master equation:

$$\begin{aligned}\dot{\rho}(t) = {} & \Gamma_A c_{X0} \rho(t) c_{X0}^{\dagger} + (\Gamma_A + \Gamma_B)/2 (c_{X0} \rho(t) c_{0X}^{\dagger} e^{i(\omega_B - \omega_A)t} \\ & + c_{0X} \rho(t) c_{X0}^{\dagger} e^{-i(\omega_B - \omega_A)t}) + \Gamma_B c_{0X} \rho(t) c_{0X}^{\dagger} \\ & - \frac{1}{2}\{c_{X0}^{\dagger} c_{X0} + c_{0X}^{\dagger} c_{0X}, \rho(t)\},\end{aligned} \tag{47}$$

where the decay rates of the two dots are given by $\Gamma_{A,B} = 2\pi \Sigma_{\mathbf{k}} |g_{\mathbf{k}}|^2 \delta(\omega_{\mathbf{k}} - \omega_{A,B})$. If $(\omega_B - \omega_A) \gg (\Gamma_A + \Gamma_B)/2$ the fast oscillating terms may be neglected as their contribution would average to zero on the time scale of the relaxation. In this case, all coherence is lost during the monitored relaxation. Therefore, for a nondestructive measurement, we must work in a regime where $(\omega_B - \omega_A) \ll (\Gamma_A + \Gamma_B)/2$. This condition is equivalent to requiring that there is a large overlap of the two spectral lines from the two quantum dots so that the two dots are to a high degree spectrally indistinguishable.

We may make a further assumption to simplify the analysis: the decay rates $\Gamma_{A,B}$ are proportional to $\omega_{A,B}^3$, and so if the detuning is small we may assume that the decay rates are identical for the two dots, i.e., $\Gamma_A = \Gamma_B = \Gamma$. The resulting master equation back in the Schrödinger picture is then

$$\begin{aligned}\dot{\rho}(t) = {} & -i[H_{\mathrm{CQD}}, \rho] + \Gamma (c_{0X} + c_{X0}) \rho (c_{0X}^{\dagger} + c_{X0}^{\dagger}) \\ & - \frac{\Gamma}{2}\{c_{X0}^{\dagger} c_{X0} + c_{0X}^{\dagger} c_{0X}, \rho\}.\end{aligned} \tag{48}$$

To derive the conditional master equation, we identify the jump operator associated with a photon detection event. As we are assuming that our detector covers the full 4π solid angle, our jump operator is simply $\mathcal{J}[\rho(t)] = \Gamma(c_{0X} + c_{X0}) \rho (c_{0X}^{\dagger} + c_{X0}^{\dagger})$. Assuming some loss in the detection process, again parametrized by the variable η, the unnormalized CME is

$$\dot{\tilde{\rho}} = -i[H_{\mathrm{CQD}}, \tilde{\rho}] + (1 - \eta)\mathcal{J}\tilde{\rho} - \mathcal{A}\tilde{\rho}, \tag{49}$$

where $\mathcal{A}\tilde{\rho} = \frac{\Gamma}{2}\{c_{X0}^{\dagger} c_{X0} + c_{0X}^{\dagger} c_{0X}, \rho\}$.

We see that when a photon is detected at a time t_D, a phase of $e^{i(\omega_A - \omega_B)t_D}$ is introduced between the $|01\rangle$ and $|10\rangle$ states. This phase is the relative phase accumulated during the time that the system spends in the excitonic levels. This is a general problem exhibited by many optical-matter-measurement-based schemes. Although, in theory we could have information about the relative phase introduced between the two levels, in practice this information can be beyond our reach, and effectively introduces a random phase. Such a random phase will destroy any coherence between the two states in the odd subspace, thereby destroying the nondestructive parity measurement.

In order to retain coherence during the measurement, we therefore require a photon detector with good enough time resolution that we are able to successfully access this phase information. If this is possible, then we may correct for the phase accumulated using single-qubit rotations, for example with a single Z rotation on the first QD.

In the worst-case scenario of distinguishable dots, we have a probabilistic scheme for generating entanglement, which is successful only when we project into the even subspace. However, this still provides a powerful resource, which is comparable with many of the existing, inherently probabilistic, schemes for measurement-induced entanglement generation.[7,8]

VI. EXPERIMENTS

We will conclude by presenting a discussion of experimental procedures for testing the fidelity of the parity measurement. Quantum process tomography provides a general procedure for characterizing the dynamics of a quantum system provided that we can measure each qubit independently in the X, Y, and Z bases. However, in our system, we must restrict ourselves to only measuring both qubits in the same basis at the same time since the two dots are not each individually addressable, and we may only perform global single-qubit rotations.

We first introduce entanglement witnesses for the four possible entangled Bell states. It has recently been shown that entanglement witnesses can be constructed for highly entangled states using the stabilizers that define these states.[28] An observable S_k is a stabilizer for the state $|\psi\rangle$ if

$$S_k |\psi\rangle = |\psi\rangle. \tag{50}$$

The stabilizers for the four Bell states are then

$$\begin{array}{cc} \text{Bell States} & \text{Stabilizers } S_k \\ |\psi_+\rangle = \frac{1}{\sqrt{2}}(|01\rangle + |10\rangle) & -Z_1Z_2, X_1X_2 \\ |\psi_-\rangle = \frac{1}{\sqrt{2}}(|01\rangle - |10\rangle) & -Z_1Z_2, -X_1X_2 \\ |\phi_+\rangle = \frac{1}{\sqrt{2}}(|00\rangle + |11\rangle) & Z_1Z_2, X_1X_2 \\ |\phi_-\rangle = \frac{1}{\sqrt{2}}(|00\rangle - |11\rangle) & Z_1Z_2, -X_1X_2 \end{array}.$$

By making measurements on XX and ZZ we are able to distinguish between the four Bell states. The ZZ measurement is related to the parity projection operators by $P_{E,O} = \frac{I \pm Z_1Z_2}{2}$. Meanwhile the XX measurement is achieved by first performing a Hadamard gate on each qubit, and then performing the same spin-parity measurement. This XX measurement effectively measures the phase between the states within each subspace. We, therefore, are using repeated applications of the parity measurement to gain information about its own operation.

As we have seen from the previous analysis (Sec. V), the primary error source in this system is decoherence between the states in the odd subspace due to distinguishability of the dots. We can, therefore, assume that there is some loss of coherence after the parity measurement, as follows:

$$P_O \rho P_O^\dagger = P_{01}\rho P_{01}^\dagger + \alpha P_{01}\rho P_{10}^\dagger + \alpha P_{10}\rho P_{01}^\dagger + P_{10}\rho P_{10}^\dagger,$$

$$P_E \rho P_E^\dagger = (P_{00} + P_{11})\rho(P_{00}^\dagger + P_{11}^\dagger). \quad (51)$$

where $P_i = |i\rangle\langle i|$. α denotes the degree of coherence; it takes a value of unity for indistinguishable dots, and will be somewhat less than that for distinguishable dots.

Starting with an initial state that is an equal superposition of the four computational states, the state of the system conditioned on observing a photon is

$$\rho_I = \frac{1}{2}\begin{pmatrix} 0 & 0 & 0 & 0 \\ 0 & 1 & \alpha & 0 \\ 0 & \alpha & 1 & 0 \\ 0 & 0 & 0 & 0 \end{pmatrix}. \quad (52)$$

Then after the global Hadamard rotation, the state is

$$\rho_{II} = \frac{1}{4}\begin{pmatrix} 1+\alpha & 0 & 0 & -1-\alpha \\ 0 & 1-\alpha & \alpha-1 & 0 \\ 0 & \alpha-1 & 1-\alpha & 0 \\ -1-\alpha & 0 & 0 & 1+\alpha \end{pmatrix}. \quad (53)$$

Finally, the probability of projecting into the odd subspace after the second parity measurement is $\frac{1-\alpha}{2}$. We, therefore, see that any loss of coherence during the parity measurements will manifest itself in the final probability, thus, giving us a clear method to quantify the effect of distinguishability on the nondestructive nature of the parity measurement.

VII. CONCLUSIONS

In conclusion, we have examined a scheme for implementing a spin-parity measurement on a pair of coupled quantum dots. We have estimated the fidelity of the parity measurement scheme presented here in the presence of realistic sources of errors. We find that the measurement is robust in the presence of inefficient detectors, ineffective spin-selective excitation, and spatial separation of the dots. For spectrally separated dots, it is found that the performance of the measurement is dependent on the degree of overlap of the spectral lines from the two dots; total spectral distinguishability results in a probabilistic measurement. Finally, we have proposed an experimental method that is able to verify the success of the parity measurement and quantify the degree to which the measurement can be performed in a nondestructive manner.

*avinash.kolli@materials.ox.ac.uk

[1] M. Kroutvar, Y. Ducommun, D. Hess, M. Bichler, D. Schuh, G. Abstreiter, and J. J. Finlay, Nature (London) **432**, 81 (2004).
[2] J. M. Elzerman, R. Hanson, L. H. W. V. Bereven, B. Witkamp, L. M. Vandersypen, and L. P. Kouwenhoven, Nature (London) **430**, 431 (2004).
[3] J. R. Petta, A. C. Johnson, J. M. Taylor, E. A. Laird, A. Yacoby, M. D. Lukin, C. M. Marcus, M. P. Hanson, and A. C. Gossard, Science **309**, 2180 (2005).
[4] D. Loss and D. P. DiVincenzo, Phys. Rev. A **57**, 120 (1998).
[5] C. Cabrillo, J. I. Cirac, P. García-Fernández, and P. Zoller, Phys. Rev. A **59**, 1025 (1999).
[6] E. Knill, R. Laflamme, and G. J. Milburn, Nature (London) **409**, 46 (2001).
[7] Y. L. Lim, A. Beige, and L. C. Kwek, Phys. Rev. Lett. **95**, 030505 (2005).
[8] S. D. Barrett and P. Kok, Phys. Rev. A **71**, 060310(R) (2005).
[9] J. Metz, C. Schon, and A. Beige, Phys. Rev. A **76**, 052307 (2007).
[10] D. L. Moehring, P. Maunz, S. Olmschenk, K. C. Younge, D. N. Matsukevich, L.-M. Duan, and C. Monroe, Nature (London) **449**, 68 (2007).
[11] B. M. Terhal and D. P. DiVincenzo, Phys. Rev. A **65**, 032325 (2002).
[12] C. W. J. Beenakker, D. P. DiVincenzo, C. Emary, and M. Kindermann, Phys. Rev. Lett. **93**, 020501 (2004).
[13] H. Engel and D. Loss, Science **309**, 586 (2005).
[14] S. D. Barrett and T. M. Stace, Phys. Rev. B **73**, 075324 (2006).
[15] A. Kolli, B. W. Lovett, S. C. Benjamin, and T. M. Stace, Phys. Rev. Lett. **97**, 250504 (2006).
[16] E. A. Laird, J. R. Petta, A. C. Johnson, C. M. Marcus, A. Yacoby, M. P. Hanson, and A. C. Gossard, Phys. Rev. Lett. **97**, 056801 (2006).
[17] B. W. Lovett, A. Nazir, E. Pazy, S. D. Barrett, T. P. Spiller, and G. A. D. Briggs, Phys. Rev. B **72**, 115324 (2005).
[18] H. Wiseman, Ph.D. thesis, University of Queensland, 1994.
[19] C. W. Gardiner and P. Zoller, *Quantum Noise* (Springer, New York, 2000).

[20] T. M. Stace, G. J. Milburn, and C. H. W. Barnes, Phys. Rev. B **67**, 085317 (2003).
[21] D. Birkedal, K. Leosson, and J. M. Hvam, Phys. Rev. Lett. **87**, 227401 (2001).
[22] E. Biolatti, I. D'Amico, P. Zanardi, and F. Rossi, Phys. Rev. B **65**, 075306 (2002).
[23] B. W. Lovett, J. H. Reina, A. Nazir, and G. A. D. Briggs, Phys. Rev. B **68**, 205319 (2003).
[24] P. Borri, W. Langbein, S. Schneider, U. Woggon, R. L. Sellin, D. Ouyang, and D. Bimberg, Phys. Rev. Lett. **87**, 157401 (2001).
[25] M. A. Nielsen and I. L. Chuang, *Quantum Computation and Quantum Information* (Cambridge University Press, Cambridge, 2000).
[26] M. Bayer, A. Kuther, A. Forchel, A. Gorbunov, V. B. Timofeev, F. Schafer, J. P. Reithmaier, T. L. Reinecke, and S. N. Walck, Phys. Rev. Lett. **82**, 1748 (1999).
[27] J. M. Luttinger and W. Kohn, Phys. Rev. **97**, 869 (1955).
[28] G. Toth and O. Guhne, Phys. Rev. A **72**, 022340 (2005).